A phenazine-based conjugated microporous polymer as a high performing cathode for aluminium–organic batteries†

Rebecca Grieco, [ID] [a] Olivera Luzanin, [ID] [bc] Diego Alvan,[a] Marta Liras, [ID] [d] Robert Dominko, [ID] [bce] Nagaraj Patil, [ID] [a] Jan Bitenc [ID] *[bc] and Rebeca Marcilla [ID] *[a]

One of the possible solutions to circumvent the sluggish kinetics, low capacity, and poor integrity of inorganic cathodes commonly used in rechargeable aluminium batteries (RABs) is the use of redox-active polymers as cathodes. They are not only sustainable materials characterised by their structure tunability, but also exhibit a unique ion coordination redox mechanism that makes them versatile ion hosts suitable for voluminous aluminium cation complexes, as demonstrated by the poly(quinoyl) family. Recently, phenazine-based compounds have been found to have high capacity, reversibility and fast redox kinetics in aqueous electrolytes because of the presence of a C=N double bond. Here, we present one of the first examples of a phenazine-based hybrid microporous polymer, referred to as IEP-27-SR, utilized as an organic cathode in an aluminium battery with an $AlCl_3$/EMIMCl ionic liquid electrolyte. The preliminary redox and charge storage mechanism of IEP-27-SR was confirmed by *ex situ* ATR-IR and EDS analyses. The introduction of phenazine active units in a robust microporous framework resulted in a remarkable rate capability (specific capacity of 116 mA h g^{-1} at 0.5C with 77% capacity retention at 10C) and notable cycling stability, maintaining 75% of its initial capacity after 3440 charge–discharge cycles at 1C (127 days of continuous cycling). This superior performance compared to reported Al//n-type organic cathode RABs is attributed to the stable 3D porous microstructure and the presence of micro/mesoporosity in IEP-27-SR, which facilitates electrolyte permeability and improves kinetics.

[a]Electrochemical Processes Unit, IMDEA Energy Institute, Avda. Ramón de La Sagra 3, 28935 Móstoles, Spain. E-mail: rebeca.marcilla@imdea.org

[b]National Institute of Chemistry, Hajdrihova 19, 1000, Ljubljana, Slovenia. E-mail: jan.bitenc@ki.si

[c]Faculty of Chemistry and Chemical Technology, University of Ljubljana, Večna pot 113, 1000 Ljubljana, Slovenia

[d]Photoactivated Processes Unit, IMDEA Energy Institute, Avda. Ramón de La Sagra 3, 28935 Móstoles, Spain

[e]Alistore-European Research Institute, CNRS FR 3104, Hub de L'Energie, Rue Baudelocque, 80039 Amiens, France

† Electronic supplementary information (ESI) available: Collected additional graphs and a table with some examples from the state of-the art. See DOI: https://doi.org/10.1039/d3fd00132f

1. Introduction

Today, the ever-growing need for electrochemical energy storage is causing more disruption to an already fragile supply chain.[1,2] As a result, more abundant and sustainable materials are sought to meet increasing battery demand. The rechargeable aluminium battery (RAB) is a new electrochemical energy storage technology that holds great promise owing to the high natural abundance of aluminium (Al), and its cost-effectiveness, safety, and sustainability. Further-more, due to its low atomic weight (26.98 g mol^{-1}) and high density (2.7 g cm^{-3}), the Al metal anode could afford high theoretical gravimetric (2980 mA h g^{-1}) and volumetric capacities (8046 mA h cm^{-3}), at a reasonably low redox potential (1.66 V $vs.$ SHE). The development of chloroaluminate ionic liquids (CILs), enabling reversible Al electrodeposition/dissolution, marked a milestone in the development of secondary RABs. In fact, these CIL electrolytes have been used in most rechargeable Al-based batteries reported so far and are considered the standard electrolyte in this technology.

Based on their redox mechanism and the nature of the active charge carrier species, two main groups of RABs can be recognised: cation-type RABs, which are based on oxide/sulfur transition metal (TM) cathodes, and anion-type RABs, such as graphite-based Al-ion batteries.[3] The first group encompasses TM oxides ($e.g.$, V_2O_5 and TiO_2)[4,5] and chalcogenides ($e.g.$, Chevrel phases)[6] that enable the (de) insertion of (chloro) aluminium cations.[7] These cation-type RABs offer high theoretical capacities, but are limited by a slow solid-state diffusion process that implies very low charge/discharge current densities.[6] Moreover, inevitable volume expansion/contraction accompanying the insertion process of large cations leads to a rather short cycle life of such batteries.[6–8] To date, the most widespread Al battery is constructed using a graphite positive electrode whose working mech-anism is based on the reversible (de)intercalation of $AlCl_4^-$ anions in the graphite structure, resulting in an anion-type RAB.[9–11] Although graphite cathodes demonstrate good rate capability and cyclability, the energy density of the full cell is limited by the intercalation of $AlCl_4^-$ anions into the graphite. Consequently, the energy density of RABs relies primarily on the amount of $AlCl_3$-based elec-trolyte, rather than the Al-metal anode.[10] It is important to note that in both battery configurations, the electrochemical reaction on the negative electrode remains the same: the reversible Al plating/stripping from $Al_2Cl_7^-$ anion species.

Recently, organic-based Al batteries, a new category of RABs, have emerged, featuring redox-active organic compounds as cathodes that exhibit 'n-type' (cation compensation) and/or "p-type" (anion compensation) behaviour. In addition to the unique ion coordination mechanism that makes them universal ion hosts,[12,13] organic materials have sparked the interest of the battery community in recent years due to their pliancy and sustainability.[14] Furthermore, the redox potential, specific capacity, and stability of organic materials can be adjusted through chemical engineering, allowing these materials to be tuned for a particular application.[15–18] Despite these unique features, research on organic-based RABs has been relatively limited to date, with a primary focus on n-type quinone compounds. This interest stems from the observed high capacities and relatively fast kinetics of quinone-based compounds in Li/Na batteries.[19]

Even though these small quinone molecules exhibit high theoretical capacities in RABs, their cycling stability is compromised by their tendency to dissolve in the electrolyte.[20–22] High-molecular-weight quinone derivatives, such as benzoquinone with four bulky phthalimide groups[21] or triangular-phenanthraquinone[22] and tetradiketone macrocycles,[23] have been demonstrated to be less soluble, thus offering excellent cyclability. However, the remaining issue of the low conductivity of these compounds leads to unsatisfactory rate performance in most reported examples. For example, the tetradiketone macrocycle exhibits an initial capacity of 226 mA h g^{-1} at 100 mA g^{-1}, but when the current density is increased to 2 A g^{-1}, the capacity drops dramatically (only 36% discharge capacity retention). In contrast, the triangle-structured phenanthraquinone, as reported by Stoddart *et al.*, exhibits an initial capacity of 94 mA h g^{-1} at 20C and adequate cycling stability (56% capacity retention after 5000 cycles at 20C). However, the mass loading (0.5 mg cm^{-2}) and the active material content (30 wt%) employed to formulate the cathodes are too low for practical application.[22]

Recently, linear quinoyl polymers, including poly(anthraquinonyl sulfide) (PAQS)[24] and polyphenanthraquinone (pPQ)[20] have also been reported, showing increased cycling stability compared to their respective small molecules (93% capacity retention after more than 500 cycles of cycling at 0.5C, in the case of pPQ). Most notably, *ex situ* EDS (energy dispersive spectroscopy) and XPS2 (X-ray photoelectron spectroscopy) experiments have shown that these 'n-type' cathode materials are capable of storing cationic Al charge carriers, allowing an almost two-fold increase in practical cell energy density compared to the state-of-the-art Al–graphite batteries.[25] Although polymerization partially circumvents the high solubility of small molecules, certain issues that limit the performance of RABs still remain. First, many linear polymers and macrocycles do not possess the robustness necessary to retain capacity over prolonged cycling.[22,23,20] Moreover, the hindered access of the highly charged (chloro) aluminium cations to the redox-active centres, which affects material utilization and limits kinetics, continues to persist in many polymer-based cathodes because of their low porosity.

To address the limited cyclability of cathodes based on small molecules and linear polymers, our approach is to incorporate redox-active units in conjugated microporous polymer (CMP) backbones. In particular, we previously synthesized an anthraquinone-based 3D microporous material (named IEP-11)[26] with a stable and robust open framework that resulted in excellent stability during cycling. This robust 3D polymer network was found to be totally insoluble and stable, circumventing the low durability of the electrode even in harsh electrolytes. In addition, this polymer structure presented excellent kinetics thanks to the combination of micro/mesoporosity and high surface area, which facilitated ion diffusion both in alkaline[26] and organic electrolytes.[27]

Only very recently, a few examples of porous polymers as cathodes in Al-metal batteries have been reported. The first one is a "p-type" bipyridine-based covalent organic framework (COF), reported in 2020 by Hongyan Lu *et al.*,[28] that presented high chemical stability and facilitated transport of AlCl$_4^-$ due to its mesoporosity. However, like most 'p-type' materials, it suffers from low energy density, as a consequence of the utilisation of AlCl$_4$ anions and high required consumption of AlCl$_3$ salt. Recently, the Xinliang Feng group reported a redox-"bipolar" polyimide COF that displayed superior cyclability compared to its small-molecule analogues.[29] To our knowledge, there is only one example of an 'n-type'

hexaazatrinaphthalene-based COF that was shown to be a versatile organic cathode in several batteries (Na, K and Mg), including aluminium batteries.[30] However, only low C rates and a small number of cycles were reported when tested in Al-metal batteries.

Until now, the application of "n-type" phenazine-based materials as electrodes has been limited to non-aqueous Li batteries[31,18] and aqueous rechargeable batteries.[32–35] However, they have not been investigated in non-aqueous RABs to date. Recently, our group developed and tested a new hybrid CMP based on phenazine (named IEP-27-SR) in both acidic and alkaline aqueous electrolytes, demonstrating excellent robustness and electrochemical performance.[32] Here, we report the use of this 'n-type' CMP as an organic cathode in a RAB with an ionic-liquid-based electrolyte (AlCl$_3$/EMIMCl). Since the C=N functionalities can offer fast kinetics, owing to the presence of N atoms with a lone pair of electrons, the introduction of phenazine active units inside a rigid porous backbone guarantees fast kinetics and great capacity retention of the aluminium battery even at high current densities (77% capacity retention at 10C). Furthermore, the Al//IEP-27-SR battery exhibited exceptional cycling stability, maintaining high capacity values even after 3440 cycles at 1C. This remarkable performance translates to a 75% capacity retention after 127 days of continuous cycling, highlighting the long-lasting capabilities of the battery. In addition to demonstrating the feasibility of our hybrid porous polymer for use in RABs, we also investigated the coordination mechanism of the phenazine active unit in AlCl$_3$/ionic liquid electrolyte using *ex situ* infrared spectroscopy and EDS analyses.

2. Experimental

2.1 Materials

4-Bromoaniline (97%, Aldrich), 1-bromo-4-nitrobenzene (99%, Aldrich), potassium *tert*-butoxide (KOtBu; ≥98%, Aldrich), *N,O*-bis(trimethylsilyl)acetamide (98%, abcr), copper(I) iodide (CuI; 98%, Fluorochem), tetrakis(triphenylphosphine)palladium(0) (Pd(PPh$_3$)$_4$; 99%, abcr), 1,3,5-triethynylbenzene (>98%, abcr), reduced graphene oxide (rGO; Nanografi), single-walled carbon nanotubes (SWCNTs; Nanografi), hexadecyltrimethylammonium bromide (CTAB; ≥98%, Sigma-Aldrich) were used. Anhydrous tetrahydrofuran (THF), *N,N*-dimethylformamide (DMF), *N*-methyl-2-pyrrolidone (NMP) and 2-propanol (IPA) were purchased from Chem-Lab and used as received. Dichloromethane (CH$_2$Cl$_2$), ethyl acetate (EtOAc), ethanol (EtOH) and methanol (MeOH) were high-performance liquid chromatography (HPLC) grade, acquired from Chem-Lab and used without prior purification.

For the battery assembly, Al foil 99.99% (0.1 mm, Alfa Aesar), AlCl$_3$ 99.99% (Sigma-Aldrich), 1-ethyl-3-methylimidazolium chloride [EMIM]Cl 97% (Acros), and urea 98% (Sigma-Aldrich) were purchased. All electrochemical tests were carried out in pouch cells using molybdenum (Mo) current collectors (0.025 mm, 99.95%, Alfa Aesar).

2.2 Synthesis of phenazine-based conjugated microporous hybrid polymer

The conjugated microporous hybrid polymer based on phenazine (named IEP-27-SR, where S = SWCNT and R = rGO) was synthesized following a two-step

polymerization that combined the miniemulsion and solvothermal methods previously reported by us.[32] SWCNTs (8.10 mg) and rGO (8.10 mg) were dispersed using an ultrasonic tip in toluene (8 mL) for 10 min. Then, 2,7-dibromophenazine (**1**) (250 mg, 0.74 mmol, 1.5 eq.) and 1,3,5-triethynylbenzene (**2**) (74.05 mg, 0.49 mmol, 1 eq.) were dissolved in Et$_3$N (8 mL) and poured into the aforementioned dispersion under stirring. The subsequent suspension was sonicated, obtaining a homogeneous dispersion. The aforementioned mixture was slowly added to 50 mL of 1% aqueous CTAB solution in a beaker and later homogenised by sonication for another 10 min. This reaction mixture was then poured into a round-bottom flask, and Pd(PPh$_3$)$_4$ (22.8 mg, 0.02 mmol, 0.04 eq.) and CuI (7.51 mg, 0.04 mmol, 0.08 eq.) were added to the flask; after degasification by bubbling argon, the mixture was stirred energetically for 3 hours under an atmosphere of argon at 80 °C. The dispersion was then moved to a Teflon-lined stainless-steel autoclave and heated to 150 °C for 3 hours. The final product was filtered by vacuum filtration and washed with a large amount of Milli-Q water, MeOH, THF, and CH$_2$Cl$_2$, in that order, and then dried at 75 °C under vacuum overnight. The yield obtained from IEP-27-SR was quantitative (>99%) by weight, with a mass of 231 mg. Based on gravimetry, the final weight composition of the hybrid IEP-27-SR was estimated to be 91 : 3.5 : 3.5 : 1 : 1 (active material : SWCNTs : rGO : Pd : Cu), considering that it is not possible to remove all of the catalyst from the polymer structure.

2.3 Physical characterisation of IEP-27-SR

^{13}C NMR spectra of IEP-27-SR were recorded at 100 MHz with a Bruker instrument. Fourier transform infrared (FTIR) spectroscopy was performed on a Nicolet 6700 from Thermo Scientific. The specific surface area and pore-size distribution were determined by analysis of N$_2$ adsorption–desorption isotherms, obtained at 77 K using a QuantaChrome Autosorb iQ2. Before analysis, the sample was thoroughly dried and degassed at 100 °C for 10 hours. The specific surface area was calculated using the Brunauer, Emmett and Teller (BET) method (S_{BET}). The total pore volume (V_{tot}), micropore volume (V_{micro}), and microporous and mesoporous surface area (S_{micro}/DFT, S_{meso}/DFT) were also calculated *via* the quenched solid density functional theory (QSDFT) method using a calculation model with slit, cylindrical, and sphere pores.

The morphology of IEP-27-SR was investigated with field emission scanning electron microscopy (FESEM; JEOL JSM-7800F Prime) and transmission electron microscopy (TEM; FEI Talos F200X) imaging techniques. The SEM and TEM images were acquired operating with 15 kV and 200 kV, respectively.

2.4 Preparation of IEP-27-SR electrodes

All polymer electrodes were prepared in the form of buckypaper following a procedure described elsewhere.[27,32] As an example, for a fixed composition of 50 : 50 wt% (carbon : active material), the following protocol was applied. First, 7.5 mg of SWCNTs were dispersed in a 20 mL solution of IPA/NMP (1/1 v/v) through a probe-tip sonicator for 10 min, half power, half amplitude (ultrasonic processor UP400S, 400 W, 24 kHz). Then, 10 mg of IEP-27-SR hybrid polymer (containing 3.5% SWCNTs and 3.5% rGO) were added to the dispersed solution and the mixture sonicated with the probe tip again for 2 minutes. After

that, the dispersion was immersed in a bath sonicator (Branson 2510, 100 W, 42 kHz) for 2 h, then stirred overnight to prepare the electrode ink. To obtain a self-standing electrode, the suspension was filtered through a Nylon membrane filter (47 mm diameter, pore size 0.45 μm) with the help of a vacuum, followed by thorough rinsing with IPA. The buckypaper was carefully removed from the filter and dried overnight at 75 °C under a vacuum. The buckypaper was cut into circular discs with a diameter of 8 mm. The active material mass loading (considering the mass of the polymer without any carbon contribution) was 1 mg cm^{-2}.

2.5 Assembly of aluminium–polymer batteries

The aluminium polymer battery was assembled in pouch cell format combining IEP-27-SR buckypapers (8 mm in diameter) as cathodes with Al anodes that were obtained by cutting Al foil (16 mm in diameter). Glass fiber separators (Whatman GF/A) were used with 100 μL of electrolyte per cell. The Al electrolyte was prepared by slowly adding $AlCl_3$ to EMIMCl (1.5 : 1) with continuous stirring. Subsequently, Al foil was added to the electrolyte and mixed overnight. An alternative Al electrolyte based on a mixture of $AlCl_3$: urea = 1 : 3 was also prepared according to the reported procedure.[20]

2.6 Electrochemical characterization of IEP-27-SR

Cyclic voltammetry (CV) was performed in the potential range between 0.2 V and 1.6 V, increasing the scan rate from 0.25 up to 100 mV s^{-1}. Galvanostatic charge–discharge (GCD) experiments were carried out in the same potential window, increasing the current density from 0.5C up to 50C. CV and GCD experiments were performed with a BioLogic VMP3 multichannel potentiostat.

As a commonly used procedure for polymer-based organic batteries, the specific capacities and current rates (C-rates) were normalized with respect to the mass of the polymer (active material) in the electrode. Therefore, the mass of SWCNTs and rGO in the hybrid and the additional SWCNTs used for the preparation of the buckypapers are not considered here. The theoretical specific capacity was calculated to be 194 mA h g^{-1}, considering the repeating unit formed by one triethynylbenzene unit and 3 phenazine units that contribute to a total of 6 electrons in the redox process.

2.7 *Ex situ* analyses

The electrodes for *ex situ* measurements were discharged and charged with the current corresponding to C/2 in the potential window 0.2–1.6 V. After 2 cycles, cells were disassembled inside the glovebox in an argon atmosphere and washed three times with 5 mL of anhydrous THF. The electrodes were then left to dry inside the glovebox overnight before measurements. Infrared characterisation of the cycled electrodes was performed inside an Ar-filled glovebox to prevent degradation of the redox-active material in contact with air or moisture. ATR-IR Alpha II (Bruker) was used, and measurements were performed in the range 2000–600 cm^{-1} with a resolution of 4 cm^{-1}. SEM/EDS analyses were conducted on a FE-SEM Supra 35 VP Carl Zeiss instrument, at an accelerating voltage of 20 kV with the use of an Oxford Instruments Ultim Max 100 EDS detector. Electrodes were prepared in the same way as for the infrared measurements. The samples

were transferred in a vacuum holder from the glovebox to the microscope to prevent sample degradation in the ambient atmosphere.

3.   Results and discussion

3.1   Synthesis and chemical–physical characterisation of hybrid IEP-27-SR

A phenazine-based porous polymer in the form of a hybrid (named IEP-27-SR) was synthesized by applying a protocol consisting of a miniemulsion step followed by a solvothermal reaction step (see Fig. 1a).[32] The polymerization process, *via* the Sonogashira cross-coupling reaction, involves 2,7-dibromophenazine (1) and 1,3,5-triethylbenzene (2) as building blocks that react in the presence of SWCNTs and rGO. This reaction pathway favours intimate contact between the nanocarbons and the porous polymer within the hybrid material.[32,27] The chemical composition of hybrid IEP-27-SR was confirmed by solid-state ^{13}C NMR spectroscopy and Fourier transform infrared spectroscopy (FTIR) (see Fig. S1a and b†).[32]

The textural properties of hybrid IEP-27-SR were determined by analysing the nitrogen adsorption–desorption isotherm (Fig. 1b).[32] The isotherm has a type IV
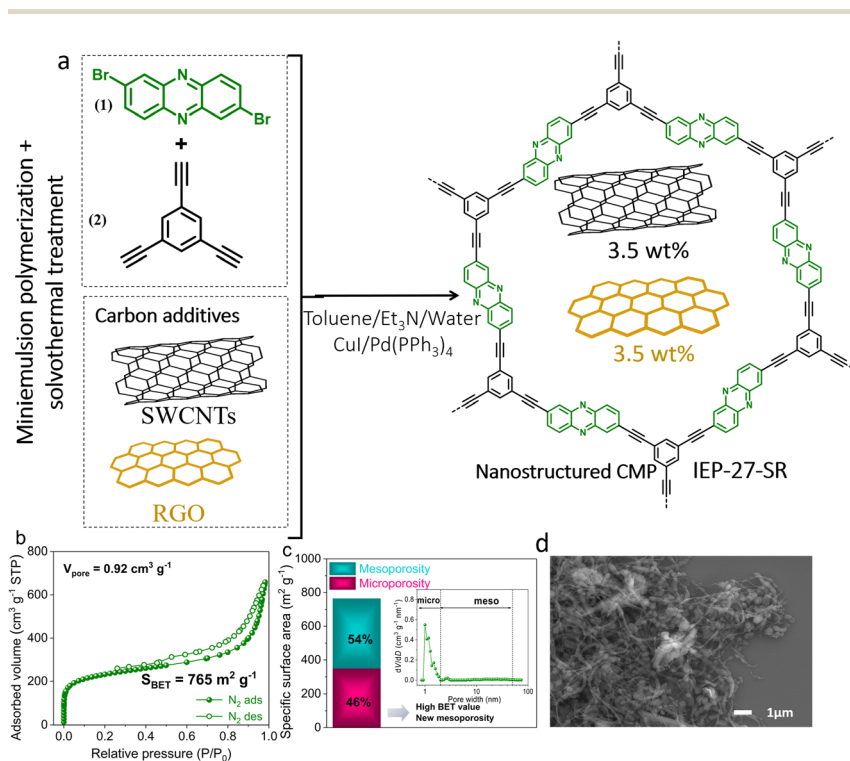

Fig. 1   (a) Synthesis scheme of the IEP-27-SR hybrid. (b) Nitrogen adsorption–desorption isotherm. (c) Percentages of micro-/mesoporosity and pore-size distribution of IEP-27-SR (inset) from the quenched solid density functional theory (QSDFT) model. (d) FE-SEM image of the IEP-27-SR hybrid. The scale bar is 1 μm.

shape, typical of mesoporous materials. The measured specific surface area (S_{BET}) is 765 m^2 g^{-1}. The distribution of the pore size was obtained from the quenched solid density functional theory (QSDFT) model and it confirmed the presence of both microporosity (46%) and mesoporosity (54%) with a total pore volume (V_{tot}) of 0.92 m^3 g^{-1} (Fig. 1c).[32]

The morphology of the polymer particles was investigated by SEM and TEM. The SEM image in Fig. 1d shows that the polymer is characterised by round-shaped nanoparticles combined with long porous nanowires, which resemble spaghetti-shaped nanostructures. From the TEM analysis (Fig. S1c†), we could assess the average round-shaped particle diameter to be around 300–400 nm, clearly characterized by a porous structure. The absence of large particle aggregates, which are typical in conventional condensation reaction routes, was also confirmed by SEM (Fig. 1d). This is attributed to the nanostructuration process that occurs during the miniemulsion synthesis step, as reported elsewhere.[36] The synergetic inclusion of the carbon additives into the polymer backbone is also evident, as the SWCNTs (wire shape) and rGO (crystalline structure) envelop the polymer particles (Fig. 1d).

3.2 Electrochemical performance of Al//IEP-27-SR

We examined the electrochemical performance of the hybrid IEP-27-SR polymer in pouch cells that were assembled using a hybrid IEP-27 buckypaper electrode as a self-standing cathode and aluminium foil as an anode. The cathode and anode were separated by a glass-fibre separator soaked with AlCl$_3$/EMIMCl electrolyte (molar ratio of 1.5 : 1), as reported elsewhere.[20,24,25] Cyclic voltammetry (CV) and galvanostatic charge–discharge (GCD) experiments were performed to determine the electrochemical performance of the newly developed phenazine-based porous polymer as a cathode for aluminium–organic batteries.

The operation of this aluminium battery during discharge/charge depends on the reversible reduction/oxidation of the phenazine active units at the cathode, and the reversible stripping/plating of Al at the anode. A general scheme of the battery and half-reactions at both the cathode and anode is represented in Fig. 2a. During the discharging process, the phenazine active units are sequentially reduced by acquiring one electron, producing a radical anion (Phz$^{\cdot-}$) that undergoes a second one-electron reduction, forming the phenazine dianion (Phz^{-2}) (Fig. 2a). To maintain the charge neutrality of the electrode, AlCl$_2^+$ is formed from Al$_2$Cl$_7^-$ as reported elsewhere,[37] according to the following equation:

$$2Al_2Cl_7^- \leftrightarrow AlCl_2^+ + 3AlCl_4^- \tag{1}$$
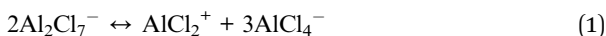
Subsequently, the negatively charged polymer backbone is coordinated by the formed cations, as observed in other n-type polymers such as quinones. Therefore, the reaction at the cathode can be expressed as follows:

$$4Al_2Cl_7^- + Phz + 2e^- \leftrightarrow Phz^{2-} \cdot 2AlCl_2^+ + 6AlCl_4^- \tag{2}$$
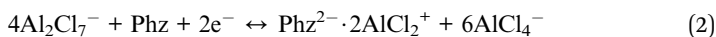
Concurrently, Al metal is stripped from the anode through AlCl$_4^-$/Al$_2$Cl$_7^-$ disproportion during discharge, according to the following half-reaction:
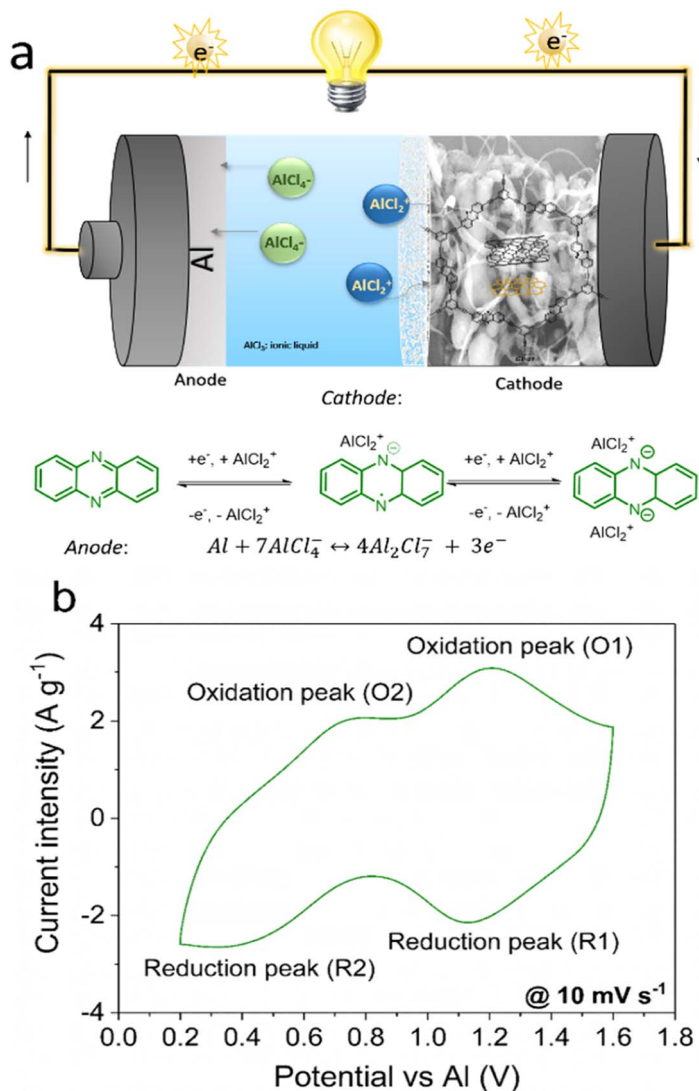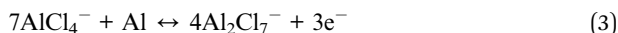
Fig. 2 (a) Scheme of the aluminium–phenazine battery during discharge and general redox working mechanism of the phenazine unit and Al reactions. (b) CV recorded at 10 mV s^{-1} illustrating the two sequential one-electron and one-AlCl$_2{}^+$ redox reaction steps.

$$7AlCl_4^- + Al \leftrightarrow 4Al_2Cl_7^- + 3e^- \tag{3}$$

During the charging step, the reverse reactions take place.

Fig. 2b shows the cyclic voltammetry of the Al//IEP-27-SR cell in the selected IL electrolyte in a potential window of 0.2–1.6 V. The CV shows two pairs of reversible redox peaks located at around 1.1 V (peaks O1 and R1) and around 0.6 V (peaks O2 and R2), which were assigned to the reversible reduction/oxidation of the phenazine moiety in the polymer structure. Considering the phenazine redox

mechanism, the presence of the two pairs of peaks is attributed to the reduction of the C=N bonds with the subsequent coordination of cationic chloroaluminate ions in two consecutive one-electron reaction steps, as discussed in the previous paragraph. An analogous mechanism with similar CV features has also been observed with phenazine small molecules in aprotic electrolytes, where it was attributed to two consecutive one-electron reactions.[18]

After confirming the reversible redox behaviour of IEP-27-SR, the kinetics of this electrochemical process were investigated by performing CV at different scan rates. When scan rates increased, a progressive separation between the redox potential of the cathodic and anodic peaks is observed, as shown in Fig. 3a. However, the peak-to-peak potential separation remains small (less than 200 mV) for all scan rates, indicating that IEP-27-SR experiences fast kinetics in the $AlCl_3$ ionic-liquid electrolyte. Since the measured current (i_p) and the scanning rate (v) obey the power-law relationship (eqn (4)),

$$i_p = av^b \tag{4}$$

where a and b are adjustable coefficients, we could apply power law analysis to determine the exponential b-value, considering the slope of the linear plot of log i_p versus log v (Fig. 3b and c). When $b = 1$, the electrode exhibits a characteristic capacitive-controlled behaviour, while a b-value of 0.5 indicates a diffusion-controlled process.[38,39] In this case, the b values for the first anodic/cathodic
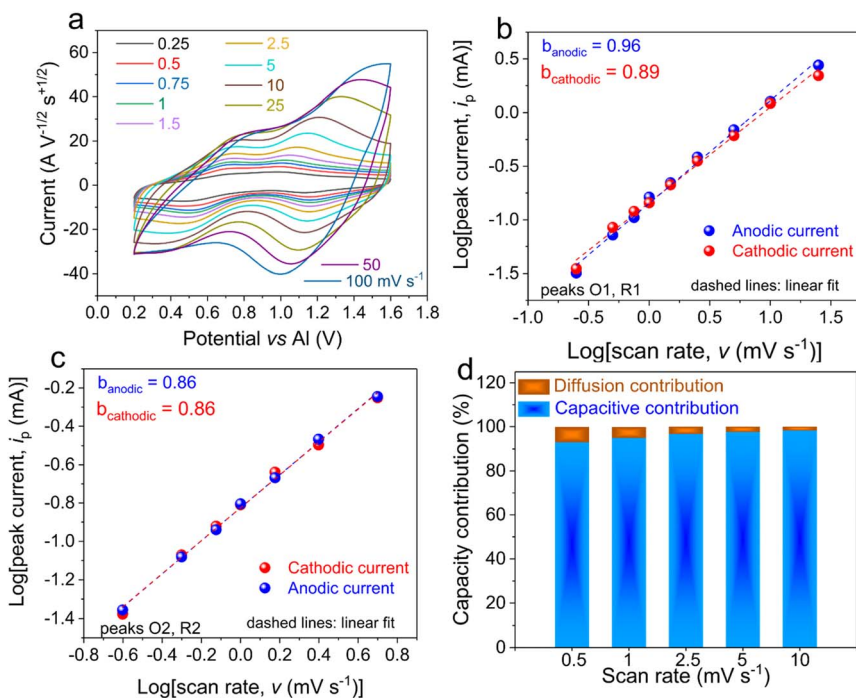

Fig. 3 (a) CVs at different scan rates for the Al//IEP-27-SR cell. (b) Power-law analysis for the peaks O1 and R1. (c) Power-law analysis for the peaks O2 and R2. (d) Capacitive contribution and diffusion contribution to the total capacity at different scan rates.

peaks (O1 and R1, around 1.1 V) were found to be 0.96/0.89, whereas the b values were 0.86/0.86 for the second peaks (O2 and R2, around 0.6 V). This evidenced the fast kinetics of the IEP-27-SR hybrid in the $AlCl_3$/EMIMCl electrolyte, which is characterized by a capacitance-controlled behaviour. More specifically, the capacitive contribution and the diffusion contribution to the total capacity were calculated from the CV curves at various scan rates (Fig. 3d) using the following equation:[40]

$$i = k_1 v + k_2 v^{1/2} \tag{5}$$

where v is the scan rate and $k_1 v$ refers to the capacitive contribution and $k_2 v^{1/2}$ refers to the diffusion contribution. By determining the constants k_1 and k_2, the fraction of current from surface capacitance and the diffusion-controlled process can be distinguished for every scan rate. As observed in Fig. 3d, at the low scan rate of 0.5 mV s^{-1}, the capacitive contribution to the total capacity is as high as 93%, and this increases to 98.9% at the scan rate of 10 mV s^{-1}, as expected. The capacitance-dominated behaviour of IEP-27-SR agrees with the b-values found for both the anodic and cathodic currents and confirms the fast kinetics of the porous polymer.
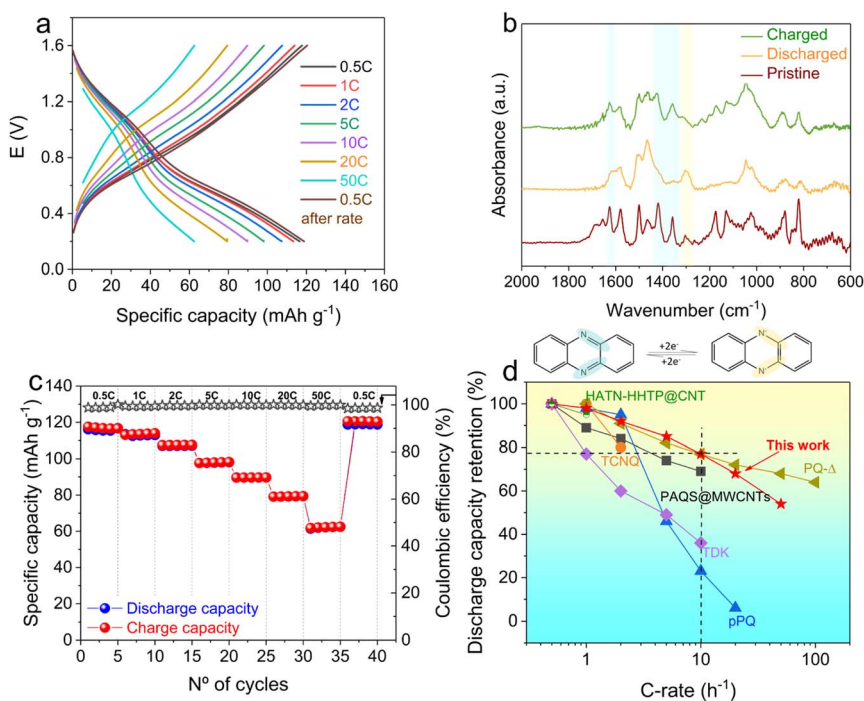

Fig. 4 (a) GCD profiles of the Al//IEP-27-SR battery at different current densities. (b) Infrared spectra of the pristine, discharged, and charged phenazine electrode and the phenazine redox mechanism. (c) Battery rate performance at different current densities and CE. (d) Performance rating and comparison of the Al//IEP-27-SR battery with representative examples of n-type polymers. All examples used for this comparison are reported in Table S2† and are listed here with the respective reference numbers: PQ-Δ,[22] PAQS@MWCNTS,[25] TCNQ,[42] HATN-HHTP@CNT,[30] TDK,[23] and ppQ.[20]

The electrochemical performance of the Al//IEP-27-SR pouch cell was evaluated by GCD at different C-rates (Fig. 4a). It is important to note that the GCD profiles, especially those obtained at low C rates (Fig. S2†), show two pairs of charge/discharge plateaus, despite their sloping nature. This is consistent with the two reversible peaks observed in the CV (Fig. 2b). The highest specific capacity value of 116 mA h g^{-1} was achieved at the lowest current density of 0.5C, with a coulombic efficiency (CE) as high as 99%. It should be noted that carbon additives alone delivered only 22 mA h g^{-1} and, for this reason, their contribution to the total capacity of the composite cathode can be considered low, despite the high carbon content (50 wt%) (see Fig. S3 and related discussion in the ESI†).

To investigate the structural changes in the phenazine-based polymer after reduction/oxidation, *ex situ* infrared spectroscopy was performed on pristine, discharged and charged electrodes (Fig. 4b and S4†). When phenazine is reduced (discharged state), the characteristic peak at 1627 cm^{-1}, corresponding to C=N stretching, decreases in intensity (Fig. 4b). This is in accordance with the electrochemical performance, as capacity utilization in the material is incomplete and the remaining C=N bonds are thus still present. In subsequent oxidation, the peak reappears, indicating the reversibility of the oxidation/reduction of the phenazine redox moiety. The change in the C=N vibration is also accompanied by several changes in the fingerprint region (*e.g.*, during polymer reduction, disappearance of peaks at 1380 cm^{-1} and 1420 cm^{-1}, which appear again during charging). Moreover, a new peak at around 1300 cm^{-1}, corresponding to the C–N–stretching, appears upon polymer reduction and disappears again upon oxidation. These changes in the infrared spectra are in good agreement with previous reports of electrode materials in aprotic lithium batteries,[18,41] where the phenazine moieties are reduced during discharge, generating anions on the polymer backbone that are coordinated by cations for charge compensation.

According to the literature, the AlCl^{2+} dication and AlCl$_2^+$ monocation, formed during battery operation, are the two main cations involved in the coordination with n-type materials.[37] Notably, there is a certain controversy in the scarce literature on aluminium–polymer batteries. Some authors claim that monovalent AlCl$_2^+$ cations serve as the charge carriers in quinone n-type polymers,[42,43] while other authors identified divalent AlCl^{2+} cations as the main charge carrier in those redox polymers.[20,25] Moreover, for pyrazine-based polymers, coordination of two different cations was reported, even though the monomer structures are very similar. A HATN-HHTP@CNT porous polymer was claimed to store AlCl^{2+} (ref. 30), but poly(hexaazatrinaphthalene) (PHATN), synthesized by Luo *et al.*, seems to coordinate AlCl$_2^+$.[44]

Although it is beyond the scope of this article to deeply investigate the complex ionic charge-storage mechanism in aluminium–phenazine batteries, we performed *ex situ* SEM/EDS analysis of pristine, charged and discharge electrodes to get some insight into the dominating ionic species in the discharged polymer. Table S1† shows that the amounts of Al and Cl in the discharged electrode after the subtraction of the unwashed compounds are around 0.7 and 1.8, respectively. This gives a ratio between Cl and Al of approximately 2.6, indicating that the main cation that coordinates the reduced hybrid polymer is likely AlCl$_2^+$. This finding aligns well with previous observations made by other researchers studying redox-active polymers.[9,22,42,43]

As expected, the C-rate capability test (Fig. 4a and c) revealed that when the current density was gradually increased, the specific capacities consequently decreased. However, the pouch cell was able to attain high values of capacity at high currents, with a discharge capacity as high as 62 mA h g^{-1} obtained at 50C. This corresponds to a capacity retention of 54% for a (dis)charging time of only 23 seconds (Fig. S5†). Additionally, when the C-rate was switched back to 0.5C, the cell recovered 100% of its initial specific capacity, showing the ability of IEP-27-SR to sustain high currents, while maintaining high electrochemical performance. Moreover, the coulombic efficiencies of higher than 98.5% for all current densities demonstrate the absence of parasitic reactions in the electrodes and the good reversibility of the aluminium–polymer battery. Considering the high cost and low sustainability of the ionic-liquid-based electrolyte,[45] we decided to perform a preliminary test of the phenazine hybrid porous polymer in a cost-effective urea–AlCl$_3$ based electrolyte (1.0 : 1.3, molar ratio)[45] (see Fig. S6†). At the current density of 0.5C, a specific capacity of 96 mA h g^{-1} is attained, demonstrating the versatility of the phenazine porous network as a cathode for Al batteries, even in the urea–AlCl$_3$-based electrolyte. However, the more sluggish plating–stripping of Al in such an electrolyte[45,46] is reflected in the overall lower performance of the battery, especially at high rates.

To highlight the advantages of the phenazine CMP in aluminium batteries, a comparison with some of the most representative n-type organic cathode materials in RABs, with the most widely used AlCl$_3$-based ionic liquid electrolyte, was performed (see Table S2†). Fig. 4d shows the capacity retention as a function of the current density (represented as $\log_{10}$ of the C-rate) of Al//IEP-27-SR, together with some examples from the state of the art. Fig. 4d reflects the excellent rate capability of the IEP-27-SR hybrid polymer, which still delivers a capacity retention of 77% at a high current density of 10C. In contrast, most reported linear polymers and macromolecules were unable to maintain high capacity values at high currents. For example, TDK showed 37% capacity retention,[23] while pPQ only retained 23% of its initial capacity at 10C (compared to the capacity at 0.5C).[20] The rate performance of pQ-Δ was slightly better than that of IEP-27-SR; however, the mass fraction and mass loading of pQ-Δ in the electrode were very low: 30 wt% and 0.5 mg cm^{-2}, respectively.[22] The excellent rate capability of the IEP-27-SR hybrid polymer, which surpasses most state-of-the-art polymers, can be attributed to two key factors. First, the three-dimensional microporous/mesoporous network guarantees easy ion accessibility and facilitates ion transport.[26] Secondly, the intimate contact between the phenazine polymer and the conductive carbon additives ensures adequate electronic conductivity of the IEP-27-SR hybrid material.[27] The combination of these features, facilitating both ionic and electronic mobilities, enables fast redox kinetics and rapid coordination between the phenazine active moieties and chloroaluminium cations, thereby further enhancing the rate performance of the pouch cell.

The cycle life is another important parameter for assessing the overall electrochemical energy storage performance of a battery. Although analysing the cyclability in terms of capacity retention per cycle is a common practice for static batteries, this parameter depends on many factors, such as cycle rate, mass loading, depth of charge/discharge, temperature, *etc.* Therefore, using this term to compare the cycle life of electrodes tested under different conditions is not straightforward, since the stability of an electrode material might also depend on

the duration of the cycling experiment, somehow nullifying the cycling rate factor, at least to some extent. To overcome this issue, a temporal metric, such as the capacity fade per day, has been recently established as more appropriate to evaluate the cycle life in certain batteries, such as redox flow batteries. Here, we evaluated the long-term stability of IEP-27-SR in the Al battery at 1C over 3440 cycles (see Fig. 5 and S7†) and analysed the capacity retention, normalizing by number of cycles (%/cycle) and by experiment duration (%/day). As observed in Fig. 5a, in the first 250 cycles, the cell revealed an impressive capacity retention of 99%, displaying a capacity of 98 mA h g^{-1} (medium capacity decay fade of 0.0059 mA h g^{-1} per cycle). Although the capacity decays slightly faster over the subsequent cycles, the average capacity fade is still as low as 0.0071 mA h g^{-1} per cycle (corresponding to 0.19 mA h g^{-1} per day). This is one of the lowest values reported so far in the literature for n-type polymers in RABs (Fig. 5c). After 3440 cycles, which corresponds to 127 days of continuous cycling, cell capacity retention is still 75% (Fig. 5a and S7†). For a fair evaluation of the long-term stability of the battery,[25] we also
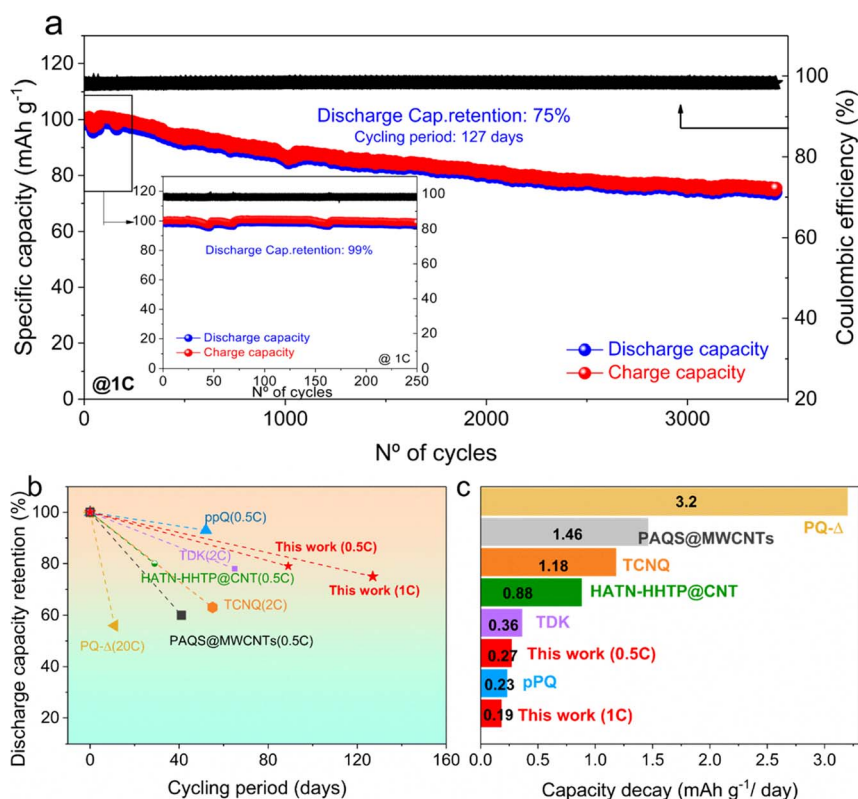

Fig. 5 (a) Long-term cycle stability of an Al//IEP-27-SR battery at 1C after 3440 cycles and after 250 cycles (inset). (b) Discharge capacity retention *vs.* number of days: comparison with some other n-type polymers reported in the literature. (c) Capacity fade per day. All examples used for this comparison are reported in Table S2† and are listed here with the respective reference numbers: PQ-Δ,[22] PAQS@MWCNTS,[25] TCNQ,[42] HATN-HHTP@CNT,[30] TDK,[23] and ppQ.[20] Details of the protocol applied for the calculation of the number of days and the corresponding fade are given in ESI.†

performed a long cyclability test at lower C-rate (0.5C), where parasitic reactions are generally exacerbated. Fig. S8† shows that the initial capacity of 116 mA h g^{-1} obtained at 0.5C slightly decreases in the first cycles; however, it stabilizes in the subsequent cycles at around 100 mA h g^{-1}. After 1000 cycles (corresponding to 89 days of cycling), a capacity retention as high as 79% is achieved, confirming the robust character of the phenazine-based conjugated microporous polymer.

Finally, we compared the stability of our Al//porous polymer cell with other Al//n-type polymer cells in terms of discharge capacity retention (%) *versus* cycling period (Fig. 5b and c) and *versus* number of cycles (Fig. S9†). The capacity losses of the IEP-27-SR cell are only 0.0071 mA h g^{-1} per cycle and 0.024 mA h g^{-1} per cycle when cycled at 1C and 0.5C, respectively (Fig. S9b†). These values are among the smallest fades reported so far. It is important to note that even if the number of cycles of our Al//IEP-27-SR cell is not the largest ever reported, the duration of the experiment, which might be considered a practical indicator of the longevity of a battery, is one of the longest reported, at more than four months (127 days). Interestingly, Fig. 5c shows that the capacity fades per day (0.19 mA h g^{-1} per day and 0.27 mA h g^{-1} per day at 1C and 0.5C, respectively) are among the lowest reported so far for n-type polymer cathodes in Al batteries.

The overall excellent rate and cycling stability performance of Al//IEP-27-SR confirms the great advantages in terms of the reversible electrochemistry, fast kinetics, mechanical integrity, low solubility and robust electrochemistry of this phenazine-based CMP in Al$_3$Cl/EMIMCl electrolyte.

4. Conclusions

Here, we assembled and characterised an Al-organic battery pouch cell with excellent rate capability and long-term cyclability using a phenazine-conjugated microporous polymer cathode (called IEP-27-SR). By providing efficient pathways for the movement of ions and electrons, the hybrid IEP-27-SR polymer allowed swift charge transfer processes, contributing to improved cell performance. Thanks to the improved kinetics and robustness of our polymer cathode, intrinsic to its structural designability, the cell not only exhibited remarkable rate capability, with 80% capacity retention at 10C while attaining 93 mA h g^{-1}, but also cycled for 127 days (corresponding to 3440 cycles), showing impressive capacity retention (75%) and a very low capacity fade of 0.19 mA h g^{-1} per day and 0.0071 mA h g^{-1} per cycle. Additionally, by employing *ex situ* ATR-IR and EDS, we could confirm the reversible redox mechanism of our polymer in the ionic-liquid electrolyte. Elemental mapping revealed that AlCl$_2^+$ was the dominant ionic species in coordination with the reduced polymer. In general, we believe that the ultrastable-phenazine cathode affirmed the versatility of organic porous polymers, even for the coordination of high-charge-density aluminium cations, where most materials undergo structural deformation and suffer from solubility issues, and may pave the way for the development of advanced multivalent batteries.

Data availability

The datasets used during the current study are available in ZENODO repository (DOI: **10.5281/zenodo.10143747**) **https://zenodo.org/records/10143747**.

Author contributions

RG, DA and ML performed the synthesis and characterization of IEP-27-SR. RG and OL performed electrochemical experiments and *ex situ* ATR-IR and EDS. RD, NP, JB and RM conceptualized the project. RM, JB and NP supervised the project. RM wrote the manuscript with assistance and contributions from all authors.

Conflicts of interest

The authors declare that they have no known competing financial interests or personal relationships that could have appeared to influence the work reported in this paper.

Acknowledgements

Notes and references

1 S. Bobba, S. Carrara, J. Huisman, F. Mathieux and C. Pavel, *Critical Raw Materials for Strategic Technologies and Sectors in the EU – a Foresight Study*, European Commission, 2020, p. 100.

2 H. Vikström, S. Davidsson and M. Höök, Lithium availability and future production outlooks, *Appl. Energy*, 2013, **110**, 252–266.

3 F. Wu, H. Yang, Y. Bai and C. Wu, Paving the Path toward Reliable Cathode Materials for Aluminum-Ion Batteries, *Adv. Mater.*, 2019, **31**(16), 1806510.

4 N. Jayaprakash, S. K. Das and L. A. Archer, The rechargeable aluminum-ion battery, *Chem. Commun.*, 2011, **47**(47), 12610–12612.

5 M. Wu, Y. Zhao, B. Sun, Z. Sun, C. Li, Y. Han, *et al.*, A 2D covalent organic framework as a high-performance cathode material for lithium-ion batteries, *Nano Energy*, 2020, **70**, 104498.

6 L. Geng, G. Lv, X. Xing and J. Guo, Reversible Electrochemical Intercalation of Aluminum in Mo6S8, *Chem. Mater.*, 2015, **27**(14), 4926–4929.

7 B. Lee, H. R. Lee, T. Yim, J. H. Kim, J. G. Lee, K. Y. Chung, *et al.*, Investigation on the Structural Evolutions during the Insertion of Aluminum Ions into Mo 6 S 8 Chevrel Phase, *J. Electrochem. Soc.*, 2016, **163**(6), A1070–A1076.

8 S. He, D. Zhang, X. Zhang, S. Liu, W. Chu and H. Yu, Rechargeable Al-Chalcogen Batteries: Status, Challenges, and Perspectives, *Adv. Energy Mater.*, 2021, **11**(29), 2100769.

9 M. C. Lin, M. Gong, B. Lu, Y. Wu, D. Y. Wang, M. Guan, *et al.*, An ultrafast rechargeable aluminium-ion battery, *Nature*, 2015, **520**(7547), 324–328.

10 D. Muñoz-Torrero, J. Palma, R. Marcilla and E. Ventosa, A critical perspective on rechargeable Al-ion battery technology, *Dalton Trans.*, 2019, **48**(27), 9906–9911.

11 K. V. Kravchyk, S. Wang, L. Piveteau and M. V. Kovalenko, Efficient Aluminum Chloride–Natural Graphite Battery, *Chem. Mater.*, 2017, **29**(10), 4484–4492.

12 C. Ding, C. Li, H. Tian, Y. Tong, W. Huang and Q. Zhang, Recent Progress on Organic Electrode Materials for Multivalent (Zn, Al, Mg, Ca) Secondary Batteries, *Batteries Supercaps*, 2022, **5**, e202200160.

13 K. Qin, J. Huang, K. Holguin and C. Luo, Recent advances in developing organic electrode materials for multivalent rechargeable batteries, *Energy Environ. Sci.*, 2020, **13**(11), 3950–3992.

14 J. J. Shea and C. Luo, Organic Electrode Materials for Metal Ion Batteries, *ACS Appl. Mater. Interfaces*, 2020, **12**(5), 5361–5380.

15 R. P. Carvalho, C. F. N. Marchiori, D. Brandell and C. M. Araujo, Tuning the Electrochemical Properties of Organic Battery Cathode Materials: Insights from Evolutionary Algorithm DFT Calculations, *ChemSusChem*, 2020, **13**(9), 2402–2409.

16 O. Allam, R. Kuramshin, Z. Stoichev, B. W. Cho, S. W. Lee and S. S. Jang, Molecular structure–redox potential relationship for organic electrode materials: density functional theory–Machine learning approach, *Mater. Today Energy*, 2020, **17**, 100482.

17 Y. Lu, Q. Zhang, L. Li, Z. Niu and J. Chen, Design Strategies toward Enhancing the Performance of Organic Electrode Materials in Metal-Ion Batteries, *Chem*, 2018, **4**(12), 2786–2813.

18 B. Tian, Z. Ding, G. H. Ning, W. Tang, C. Peng, B. Liu, *et al.*, Amino group enhanced phenazine derivatives as electrode materials for lithium storage, *Chem. Commun.*, 2017, **53**(20), 2914–2917.

19 Y. Wu, R. Zeng, J. Nan, D. Shu, Y. Qiu and S. L. Chou, Quinone Electrode Materials for Rechargeable Lithium/Sodium Ion Batteries, *Adv. Energy Mater.*, 2017, **7**(24), 1700278.

20 J. Bitenc, U. Košir, A. Vizintin, N. Lindahl, A. Krajnc, K. Pirnat, *et al.*, Electrochemical Mechanism of Al Metal–Organic Battery Based on Phenanthrenequinone, *Energy Mater. Adv.*, 2021, **2021**, 9793209.

21 Y. T. Kao, S. B. Patil, C. Y. An, S. K. Huang, J. C. Lin, T. S. Lee, *et al.*, A Quinone-Based Electrode for High-Performance Rechargeable Aluminum-Ion Batteries with a Low-Cost AlCl3/Urea Ionic Liquid Electrolyte, *ACS Appl. Mater. Interfaces*, 2020, **12**(23), 25853–25860.

22 D. J. Kim, D. J. Yoo, M. T. Otley, A. Prokofjevs, C. Pezzato, M. Owczarek, *et al.*, Rechargeable aluminium organic batteries, *Nat. Energy*, 2019, **4**(1), 51–59.

23 D. J. Yoo, M. Heeney, F. Glöcklhofer and J. W. Choi, Tetradiketone macrocycle for divalent aluminium ion batteries, *Nat. Commun.*, 2021, **12**(1), 1.

24 N. Lindahl, J. Bitenc, R. Dominko and P. Johansson, Aluminum Metal–Organic Batteries with Integrated 3D Thin Film Anodes, *Adv. Funct. Mater.*, 2020, **30**(51), 2004573.

25 J. Bitenc, N. Lindahl, A. Vizintin, M. E. Abdelhamid, R. Dominko and P. Johansson, Concept and electrochemical mechanism of an Al metal anode – organic cathode battery, *Energy Storage Mater.*, 2020, **24**, 379–383.

26 R. Grieco, A. Molina, J. S. Sanchez, N. Patil, M. Liras and R. Marcilla, A significantly improved polymer‖Ni(OH)2 alkaline rechargeable battery using anthraquinone-based conjugated microporous polymer anode, *Mater. Today Energy*, 2022, **27**, 101014.

27 A. Molina, N. Patil, E. Ventosa, M. Liras, J. Palma and R. Marcilla, Electrode Engineering of Redox-Active Conjugated Microporous Polymers for Ultra-High Areal Capacity Organic Batteries, *ACS Energy Lett.*, 2020, **5**(9), 2945–2953.

28 H. Lu, F. Ning, R. Jin, C. Teng, Y. Wang, K. Xi, *et al.*, Two-Dimensional Covalent Organic Frameworks with Enhanced Aluminum Storage Properties, *ChemSusChem*, 2020, **13**(13), 3447–3454.

29 Y. Liu, Y. Lu, A. Hossain Khan, G. Wang, Y. Wang, A. Morag, *et al.*, Redox-Bipolar Polyimide Two-Dimensional Covalent Organic Framework Cathodes for Durable Aluminium Batteries, *Angew. Chem., Int. Ed.*, 2023, **62**, e202306091.

30 S. Li, Y. Liu, L. Dai, S. Li, B. Wang, J. Xie, *et al.*, A stable covalent organic framework cathode enables ultra-long cycle life for alkali and multivalent metal rechargeable batteries, *Energy Storage Mater.*, 2022, **48**, 439–446.

31 E. Vitaku, C. N. Gannett, K. L. Carpenter, L. Shen, H. D. Abruña and W. R. Dichtel, Phenazine-Based Covalent Organic Framework Cathode Materials with High Energy and Power Densities, *J. Am. Chem. Soc.*, 2020, **142**(1), 16–20.

32 D. Alván, R. Grieco, N. Patil, A. Mavrandonakis, M. Liras and R. Marcilla, Hybrid based on Phenazine Conjugated Microporous Polymer as a High-Performance Organic Electrode in Aqueous Electrolytes, *Batteries Supercaps*, 2023, **6**(5), e202300023.

33 L. Li, L. Chen, Y. Wen, T. Xiong, H. Xu, W. Zhang, *et al.*, Phenazine anodes for ultralongcycle-life aqueous rechargeable batteries, *J. Mater. Chem. A*, 2020, **8**(48), 26013–26022.

34 T. Sun, C. Liu, J. Wang, Q. Nian, Y. Feng, Y. Zhang, *et al.*, A phenazine anode for high-performance aqueous rechargeable batteries in a wide temperature range, *Nano Res.*, 2020, **13**(3), 676–683.

35 J. Chen, Q. Zhu, L. Jiang, R. Liu, Y. Yang, M. Tang, *et al.*, Rechargeable Aqueous Aluminum Organic Batteries, *Angew. Chem.*, 2021, **133**(11), 5858–5863.

36 A. Molina, N. Patil, E. Ventosa, M. Liras, J. Palma and R. Marcilla, New Anthraquinone-Based Conjugated Microporous Polymer Cathode with Ultrahigh Specific Surface Area for High-Performance Lithium-Ion Batteries, *Adv. Funct. Mater.*, 2020, **30**(6), 1908074.

37 L. W. Gordon, J. Wang and R. J. Messinger, Revealing impacts of electrolyte speciation on ionic charge storage in aluminum-quinone batteries by NMR spectroscopy, *J. Magn. Reson.*, 2023, **348**, 107374.

38 N. Patil, C. de la Cruz, D. Ciurduc, A. Mavrandonakis, J. Palma and R. Marcilla, An Ultrahigh Performance Zinc-Organic Battery using Poly(catechol) Cathode in Zn(TFSI)2-Based Concentrated Aqueous Electrolytes, *Adv. Energy Mater.*, 2021, **11**(26), 2100939.

39 G. Fang, Z. Wu, J. Zhou, C. Zhu, X. Cao, T. Lin, *et al.*, Observation of Pseudocapacitive Effect and Fast Ion Diffusion in Bimetallic Sulfides as an Advanced Sodium-Ion Battery Anode, *Adv. Energy Mater.*, 2018, **8**(19), 1703155.

40 D. Chao, C. Zhu, P. Yang, X. Xia, J. Liu, J. Wang, *et al.*, Array of nanosheets render ultrafast and high-capacity Na-ion storage by tunable pseudocapacitance, *Nat. Commun.*, 2016, **7**, 12122.

41 X. Zhang, G. Li, J. Wang, J. Chu, F. Wang, Z. Hu, *et al.*, Revisiting the Structure and Electrochemical Performance of Poly(o-phenylenediamine) as an Organic Cathode Material, *ACS Appl. Mater. Interfaces*, 2022, **14**(24), 27968–27978.

42 F. Guo, Z. Huang, M. Wang, W.-L. Song, A. Lv, X. Han, *et al.*, Active cyano groups to coordinate AlCl2+ cation for rechargeable aluminum batteries, *Energy Storage Mater.*, 2020, **33**, 250–257.

43 L. W. Gordon, A. L. Jadhav, M. Miroshnikov, T. Schoetz, G. John and R. J. Messinger, Molecular-Scale Elucidation of Ionic Charge Storage Mechanisms in Rechargeable Aluminum-Quinone Batteries, *J. Phys. Chem. C*, 2022, **126**(33), 14082–14093.

44 M. Mao, C. Luo, T. P. Pollard, S. Hou, T. Gao, X. Fan, *et al.*, A Pyrazine-Based Polymer for Fast-Charge Batteries, *Angew. Chem., Int. Ed.*, 2019, **58**(49), 17820–17826.

45 M. Angell, C. J. Pan, Y. Rong, C. Yuan, M. C. Lin, B. J. Hwang, *et al.*, High Coulombic efficiency aluminum-ion battery using an AlCl3-urea ionic liquid analog electrolyte, *Proc. Natl. Acad. Sci. U. S. A.*, 2017, **114**(5), 834–839.

46 G. A. Elia, K. Hoeppner and R. Hahn, Comparison of Chloroaluminate Melts for Aluminum Graphite Dual-Ion Battery Application, *Batteries Supercaps*, 2021, **4**(2), 368–373.